Article

Fabrication and Characterization of a Polydopamine-Modified Bacterial Cellulose and Sugarcane Filter Cake-Derived Hydroxyapatite Composite Scaffold

Mark-Jefferson Buer Boyetey, Prakit Sukyai,* Nuntaporn Kamonsutthipaijit, Supinya Nijpanich, and Narong Chanlek

Cite This: ACS Omega 2023, 8, 43295−43303

Read Online

ACCESS | Metrics & More | Article Recommendations

ABSTRACT: The search for environmentally friendly and sustainable sources of raw materials has been ongoing for quite a while, and currently, the utilization and applications of agro-industrial biomass residues in biomedicine are being researched. In this study, a polydopamine (PDA)-modified bacterial cellulose (BC) and hydroxyapatite (HA) composite scaffold was fabricated using the freeze-drying method. The as-prepared hydroxyapatite was synthesized via the chemical precipitation method using sugarcane filter cake as a calcium source, as reported in a previous study. X-ray diffraction analysis revealed a carbonated phase of the prepared hydroxyapatite, similar to that of the natural bone mineral. Wide-angle X-ray scattering analysis revealed the successful fabrication of BC/HA composite scaffolds, while X-ray photoelectron spectroscopy suggested that PDA was deposited on the surface of the BC/HA composite scaffolds. In vitro cell viability assays indicated that BC/HA and PDA-modified composite scaffolds did not induce cytotoxicity and were biocompatible with MC3T3-E1 preosteoblasts. PDA-modified composite scaffolds showed enhanced protein adsorption capacity in vitro compared to the unmodified scaffolds. On a concluding note, these results demonstrate that agro-industrial biomass residues have the potential to be used in biomedical applications and that PDA-modified BC/HA composite scaffolds are a promising biomaterial for bone tissue engineering.
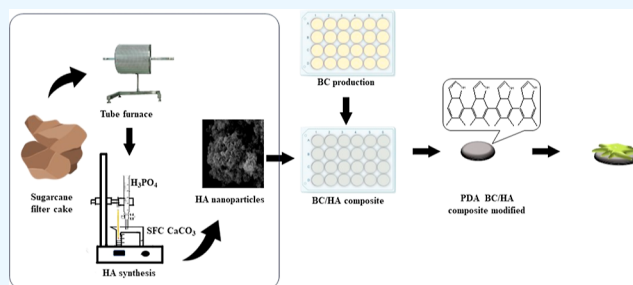
1. INTRODUCTION

The search for environmentally friendly sources of raw materials, with the goal of producing food, medicines, biologically active substances, biomaterials, and sustainable energy has been ongoing for quite a while, as petroleum and nonrenewable sources become scarce. Biomass has emerged as a sustainable alternative due to its abundance, and agro-industries generate a large amount of biomass residues which are untreated and underutilized, much of which are improperly disposed of into rivers, open fields, and landfills.[1−3] However, the past 25 years have seen significant advances in the utilization of biomass residues for bioenergy, although alternative fuels and biochar production have also increased. Currently, the upsurge in the utilization of agro-industrial biomass residues through resource recovery, particularly in bioenergy production, is primarily intended to avoid their disposal.[4]

Recently, the applications of agro-industrial biomass residues have been extended from bioenergy and packaging to biomedicine. This application encompasses usage in drug capsules, controlled release, biosensors, tissue engineering, and others due to their nontoxicity, biodegradability, and biocompatibility.[5] Additionally, as far as the chemical composition of these materials is concerned, they make valuable resources for extended usage in the production of biochemicals of biomedical importance. The use of agro-industrial biomass residues for tissue engineering is becoming more popular, with many of these experiments being carried out in the laboratory but yielding promising results. For instance, scaffolds for bone tissue engineering were fabricated from cellulose extracted from sugarcane bagasse obtained from a sugar refinery in Thailand. The fabricated scaffolds showed no evidence of toxicity to osteoblasts and supported their proliferation and differentiation in vitro.[6] Similarly, cellulose nanocrystals produced from sugarcane bagasse were utilized as a component in a poly(vinyl alcohol)-based scaffold and were
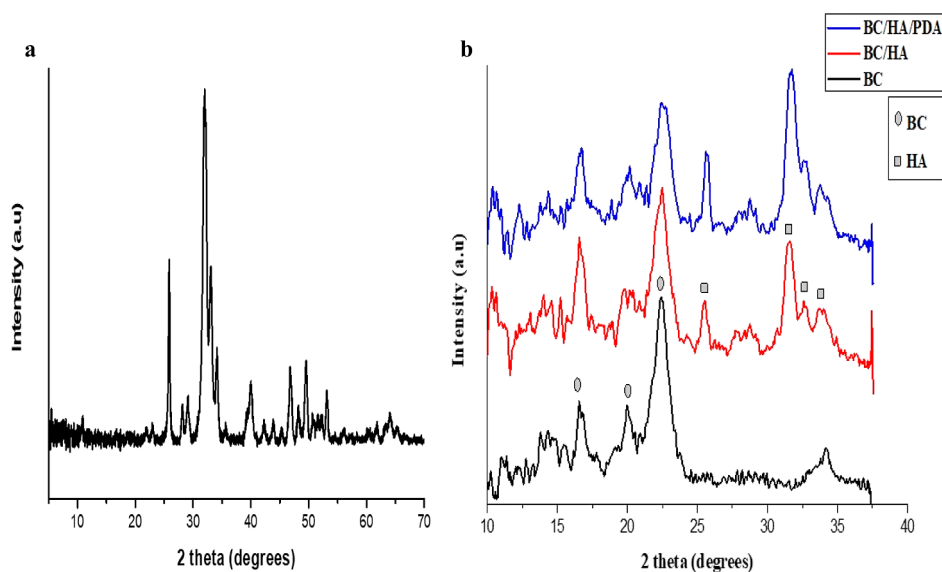
Figure 1. (a) XRD pattern of the as-prepared hydroxyapatite. (b) WAXS pattern of composite scaffolds compared with pristine BC.

evaluated for their biocompatibility with human skin fibroblasts.[7] In another study, biomolecules from the extracts of orange and potato peels were demonstrated to effectively control the morphology and size of hydroxyapatite (HA) nanoparticles. It was reported that enoic acids and limonene present in potato peels and orange peels, respectively, were crucial in controlling the nanoparticles' morphology and size.[8] In our previous study, we also successfully demonstrated the possibility of utilizing sugarcane filter cake from the sugar refinery as a source material for HA synthesis. The physicochemical characteristics of the synthesized HA were comparable to those found in bone tissue.[9]

In this study, we investigated the potential of the as-prepared HA as a constituent of a composite material for tissue engineering. HA is a bioactive ceramic with osteoinductive and osteoconductive properties, that has been reported to improve the cellular and osteogenic abilities of other materials when utilized as a component of a composite. The role of hydroxyapatite as a functional material for tissue engineering has been extensively reviewed.[10,11] Herein, bacterial cellulose (BC) was used as the main supporting structure with embedded HA nanoparticles. BC is an exopolysaccharide produced by some acetic acid-producing bacteria that functions as a protective biofilm during harsh environmental conditions, aids in their migration toward a surface oxygen-rich medium, and promotes close interaction with a preferred host.[12] Over the years, BC has been recognized as a very useful biomaterial on account of its exceptional qualities, including its biocompatibility, purity, biodegradability, and noncytotoxicity,[13] as well as its three-dimensional structure and water holding capacity. Furthermore, while BC and its composites have demonstrated suitability for a variety of tissue engineering applications, there remain opportunities to enhance their efficiencies. Among the various suitable modification alternatives, polydopamine (PDA), a bioinspired synthetic polymer coating has become one of the most effective approaches for a wide range of applications, due to its simplicity and low cost.[14,15] Furthermore, in tissue engineering, PDA modification has also been recognized to promote cell adhesion and proliferation. Thus, we fabricate and characterize polydopamine-modified bacterial nanocellulose (BC) and sugarcane

filter cake-derived HA composite scaffold as potential composite material for bone tissue engineering.

2. RESULTS AND DISCUSSION

2.1. X-ray Scattering. X-ray diffraction (XRD) analysis was performed to determine the crystalline phase of the as-prepared hydroxyapatite. The characteristic crystallographic pattern of HA was revealed, and intense peaks were observed at 2θ = 25.7, 31.8, 33.0, 34.1, 39.4, 40.0, 46.7, 49.5, and 53.1° (Figure 1a), which are similar to other reports.[16,17] A carbonate peak was also observed at 2θ = 29.0°, which makes the synthesized HA similar to the calcium phosphate mineral found in the hard tissues of animals. Carbonated HA is known to possess better resorption capacity, osteoconductivity, and solubility compared to stoichiometric HA.[18]

The wide-angle X-ray scattering (WAXS) spectra in Figure 1b present the characteristic patterns of BC/HA composite scaffolds compared with pristine BC. The characteristic diffraction peaks observed at 2θ = 16.5 and 22.4° were assigned to pristine BC, which are typical for cellulose I polymorph.[19] The peak observed at about 2θ = 19° for all samples is also a characteristic peak of cellulose type I, which is not usually observed.[20] Additional peaks were found in both BC/HA and BC/HA/PDA composite scaffolds at 2θ = 25.5, 31.6, 32.5, and 33.9 and 25.5, 31.6, 32.8, and 33.7°, respectively, which are assigned to HA. A reduction in the peak intensity at about 2θ = 22.5° was observed in the BC/HA and BC/HA/PDA composite samples, which was attributed to the deposition of HA nanoparticles on the nanofibers of BC.[21] The amorphous nature of PDA makes it lack distinguishable crystallographic characteristics.[22] This was confirmed from the WAXS spectra, as no distinct peak for PDA was observed in the BC/HA/PDA samples. The WAXS spectra showed the successful fabrication of BC/HA composite scaffolds.

3. XPS ANALYSIS

X-ray photoelectron spectroscopy (XPS) was used to examine the surface elemental composition and oxidation states of pristine BC and BC/HA composite scaffolds in the region of 0−1400 eV. The wide-scan XPS spectra (Figure 2) revealed the presence of carbon (C) and oxygen (O) for all samples.
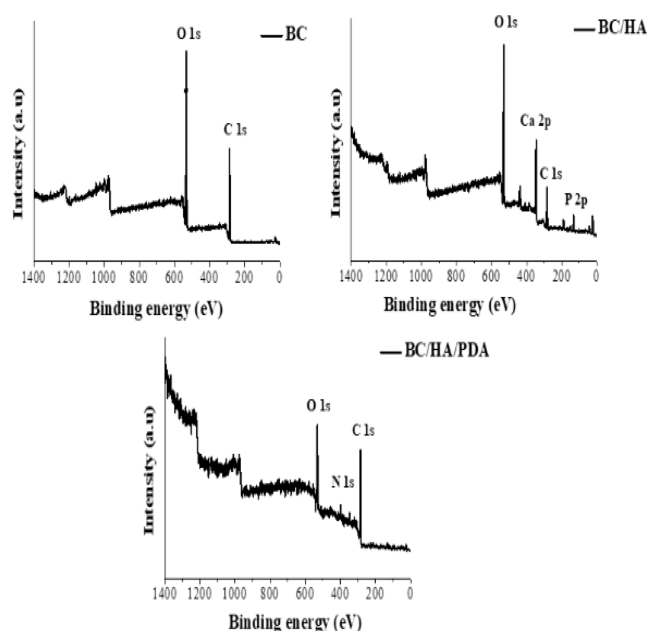
Figure 2. Wide-scan X-ray photoelectron spectra of composite scaffolds compared with those of pristine BC.

Calcium (Ca) and phosphorus (P) were found in the BC/HA and BC/HA/PDA composite scaffolds, while nitrogen (N) was detected in the BC/HA/PDA composite scaffolds only. The elemental compositions of each sample are indicated in Table 1, exhibiting percentage changes of the main atoms (C 1s, O

Table 1. Elemental Composition of Pristine Bacterial Cellulose (BC) and Bacterial Cellulose and Hydroxyapatite Composite Scaffolds

	element composition (at. %)				
sample	C	O	P	Ca	N
BC	64.23	35.77			
BC/HA	39.42	42.50	7.35	10.72	
BC/HA/PDA	66.89	23.52	0.97	1.54	7.09

1s, and P 2p) after polydopamine coating. The PDA-coated scaffolds with lower calcium and phosphorus contents had a significantly increased carbon content compared to the bare scaffolds, confirming the surface deposition of PDA. The nitrogen content obtained from the PDA-coated scaffolds is also consistent with values obtained in other reports.[23]

The high-resolution XPS spectra of C 1s and O 1s for all samples, Ca 2p and P 2p for the BC/HA composite scaffolds, and N 1s for the BC/HA/PDA composite scaffolds are shown in Figure 3. The C 1s high-resolution spectra were best fitted with four peaks, which included C−C, C−O/C−N, C=O/C=N, and O−C=O/carbonate, representing the bonds in BC and polydopamine chemical structures. These observations are similar to those reported in studies.[24−26] For pristine BC, the O 1s high-resolution spectrum was fitted into two peaks, which are assigned to O−C and O=C, whereas three deconvoluted peaks defined as O−C/P−O, O=C/P=O, and carbonates/OH were observed in the BC/HA and BC/HA/PDA composite scaffolds spectra.[27,28] The presence of carbonates in the BC/HA and BC/HA/PDA composite scaffolds is because of the carbonate element present in the HA. The high-resolution XPS spectra of the Ca 2p region for

BC/HA and BC/HA/PDA composite scaffolds were fitted with two spin−orbit doublets (Ca $2p_{1/2}$ and Ca $2p_{3/2}$), which are characteristic of calcium compounds,[29] and are assigned to the interaction between Ca ions (Ca^{2+}) and phosphate ions (PO_4^{3-}), as well as the presence of carbonates.[30,31] The P 2p high-resolution spectra present two peaks, including P $2p_{1/2}$ and P $2p_{3/2}$, which are assigned to the P−O and P=O bonds of PO_4^{3-}. The N 1s high-resolution spectrum of BC/HA/PDA was deconvoluted into three peaks (=N−, −NH−, and −NH_2), which represents the tertiary, secondary, and primary amine functionalities, respectively. The presence of the primary amine functional group is a characteristic of dopamine and dopamine quinone, while dopaminechrome relates to the tertiary amine group. The secondary amine functional group, which exhibits a higher peak intensity, denotes the presence of 5,6-dihydroxyindole and PDA. Considering the mechanism for dopamine polymerization, the high peak intensity could be attributed to increased production of 5,6-dihydroxyindole and PDA by the end of the reaction.[32,33] The PDA film was found to contain intermediates and tautomeric species, as evidenced by our findings.

3.1. FTIR Spectroscopy. Figure 4 presents the Fourier transform infrared (FTIR) spectra of pristine BC, BC/HA, and BC/HA/PDA composite scaffolds. The broad absorption band between 3200 and 3570 cm^{-1} and the peak at 2900 cm^{-1} in the single bond area of the BC spectrum were assigned to the broad band of the hydroxyl (OH) group and the stretching vibration of C−H, respectively. The deposition of HA decreased the intensity of BC's broad OH absorption band in the BC/HA composite scaffolds, which could indicate the nanocomposite stability via chemical bonds formed between BC and HA via the cellulose OH group. However, an increase in peak intensity was observed in the spectrum of BC/HA/PDA composite scaffolds due to the presence of OH groups and N−H stretching vibrations of PDA.[34] No peaks were observed in the triple bond (2500−2000 cm^{-1}) region of all samples. However, in the double bond region (2000−1500 cm^{-1}), the peak observed at 1601 cm^{-1} was assigned to the vibration of the benzene ring of PDA,[35] in the BC/HA/PDA spectrum. The fingerprint region (1500−600 cm^{-1}) showed broad peaks for all samples. However, small peaks at about 1422 and 1428 cm^{-1} observed in the spectrum of BC/HA and BC/HA/PDA composite scaffolds, respectively, were assigned to the carbonate ions (CO_3^{2-}) present in HA. The bands observed between 1100−1000 and 650−500 cm^{-1} for both BC/HA and BC/HA/PDA composite scaffolds corresponded to the stretching and bending vibrations of the phosphate ions (PO_4^{3-}) of HA, while the sharp intensity peak observed at 1050 cm^{-1} in the BC spectra was assigned to vibrations related to C−O stretching in BC. The FTIR results are in conformity with the results obtained from the XPS analysis.

3.2. Scanning Electron Microscopy. The deposition of HA on BC and its distribution in the BC cross-section, as well as the morphology of the BC/HA composite scaffold after PDA modification, are shown in Figure 5. The surfaces and cross sections of BC, BC/HA, and BC/HA/PDA were compared. Figure 5a reveals a typical smooth interlaced nanofibrous surface and cross-section of BC with an interconnected porous structure. The nanofibrous structure of BC has been reported to be ideal for nanoparticle stabilization.[21] Agglomerates of HA nanocrystals were shown to be dispersed at the surface and cross-section of BC (Figure 5b), while the 3D structure of BC was maintained. The
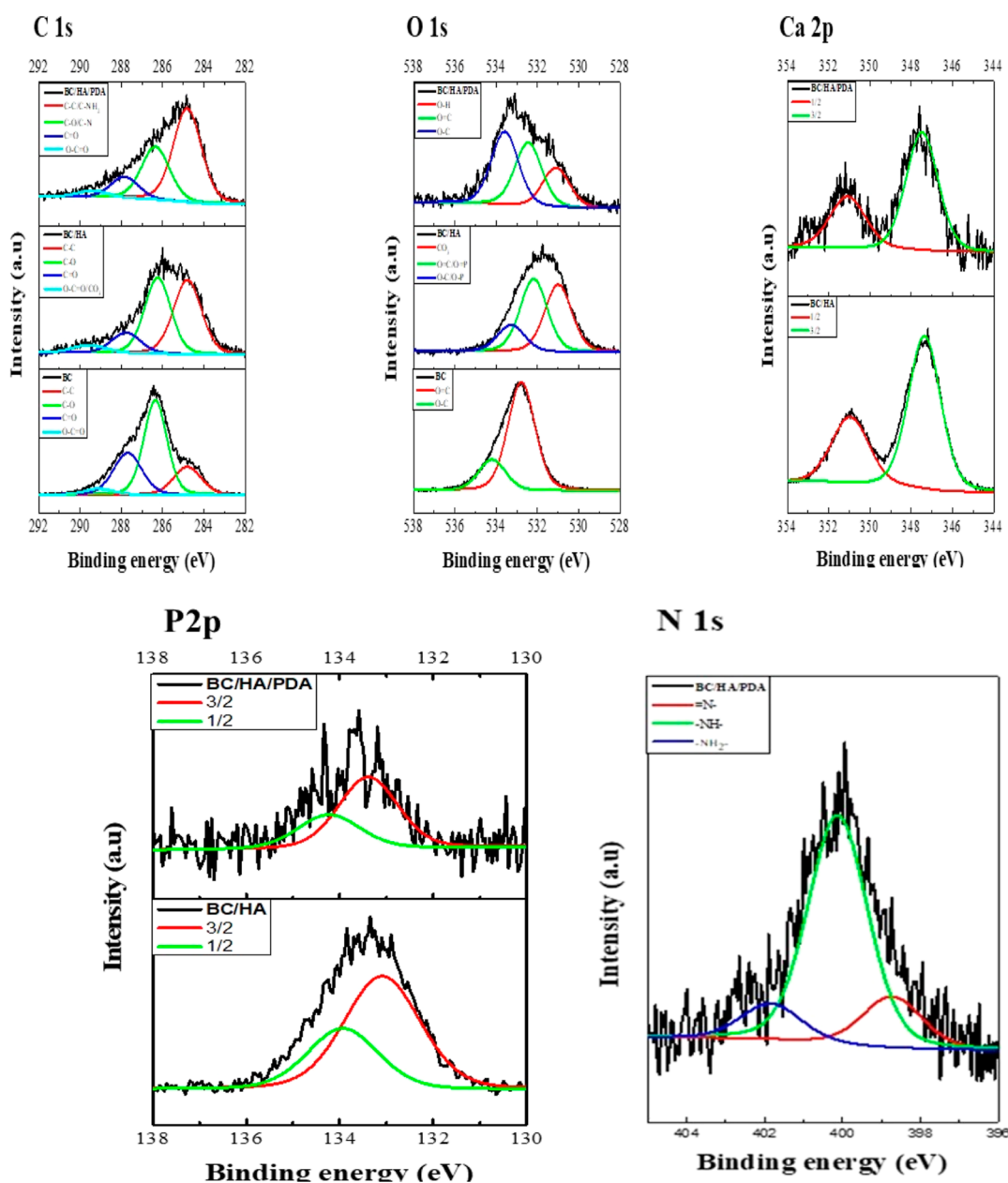
Figure 3. High-resolution X-ray photoelectron spectra of composite scaffolds compared with those of pristine BC.

interaction between the HA nanoparticles and the BC fibers is beneficial as it increases the composite's mechanical properties and osteoconductive characteristics. BC/HA/PDA showed numerous particles in comparison to BC/HA (Figure 5c) which is attributed to the deposition of PDA nanoparticle aggregates onto the surface of the BC/HA composite scaffold. The increased substrate immersion time during PDA coating results in the formation of these nanoparticles, which increases the surface roughness of the composite scaffold.[15]

3.3. Cell Viability. The cell viability results of BC/HA and BC/HA/PDA are shown in Figure 6. The samples were recognized as nontoxic in accordance with the ISO 10993−5, 2009 regulations as cell viability was above 70% for each sample. The findings of this study corroborate previous evaluations of BC and hydroxyapatite composite scaffolds that found them to be nontoxic.[36,37] The nontoxicity of PDA-modified scaffolds also supports previous reports in which PDA was used as a coating material on other substrates.[38,39]

The stability of the PDA coating on the scaffolds is also demonstrated by the fact that no cytotoxic chemicals were released from the PDA-modified scaffolds. The live/dead cell staining images also show qualitatively the effect of the scaffold extracts on the MC3T3-E1 preosteoblasts. The living cells (green fluorescence) were the dominant population of seeded cells in the BC/HA and BC/HA/PDA groups, similar to the control image, which is an indication of no cytotoxicity.

3.4. Cell Adhesion and Biocompatibility. The adhesion of MC3T3-E1 cells to the scaffolds after 24 h of culture is depicted in Figure 7. The SEM images revealed a well-spread morphology with extended pseudopodia of MC3T3-E1 cells anchored on the surface of BC/HA and BC/HA/PDA scaffolds. Moreover, filopodia are also observed at the lamellipodia, facilitating cell-to-cell interaction, which is often vital for tissue regeneration processes. It is crucial for most tissue engineering applications that cells adhere to scaffolds and remain viable. Cell-to-scaffold interactions affect cell
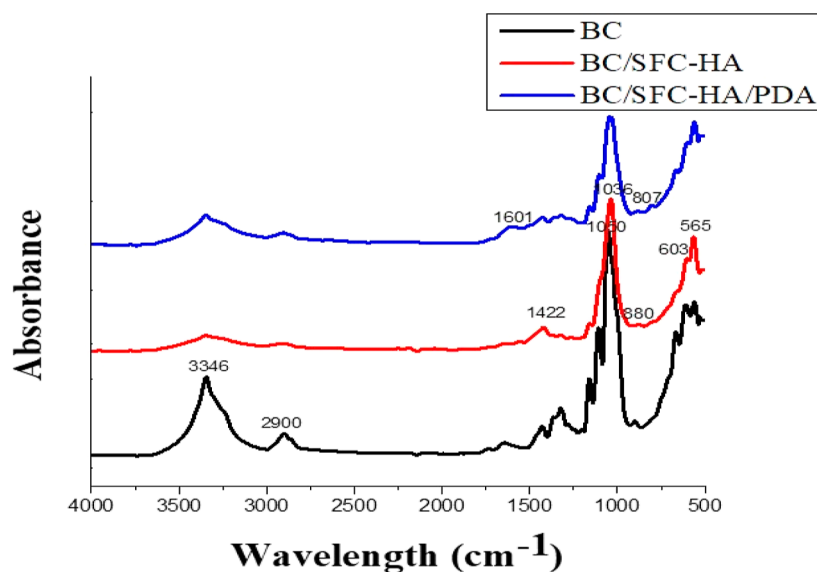
Figure 4. FTIR of composite scaffolds compared to pristine BC.
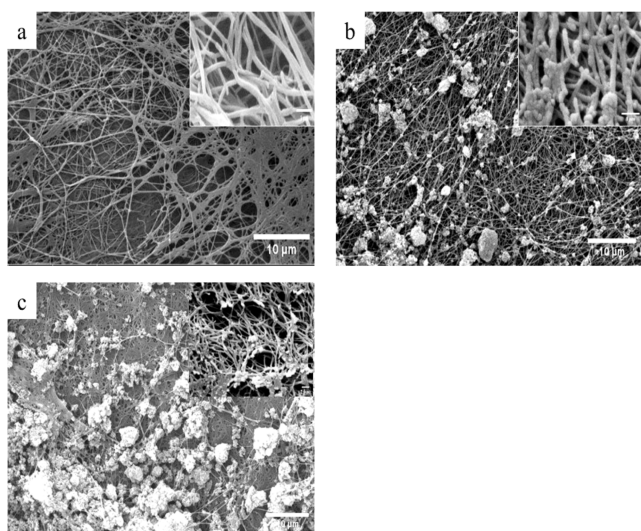
Figure 5. SEM images of (a) BC, (b) BC and hydroxyapatite composite scaffold, and (c) polydopamine-modified BC and hydroxyapatite composite scaffold, with the cross-sectional image of each sample at the top right corner.
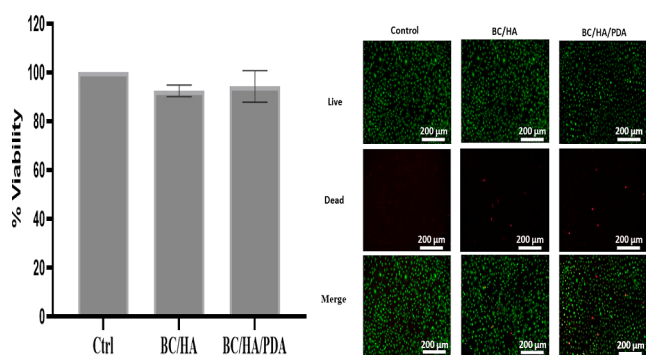
Figure 6. Quantitative and qualitative analysis of the effect of scaffold extracts on MC3T3-E1 preosteoblasts.

adhesion and morphology while also influencing other cellular processes such as migration within the scaffold, differentiation,
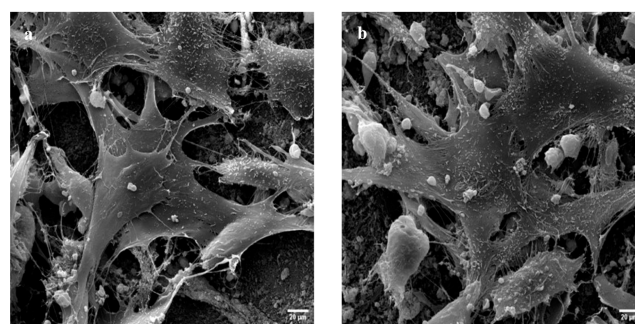
Figure 7. Cell adhesion and morphology of MC3T3-E1 cells on a (a) BC and hydroxyapatite composite scaffold and (b) polydopamine-modified BC and hydroxyapatite composite scaffold.

and mechanical cues transduction to the cells.[40] The physicochemical characteristics of materials are one of the several factors that influence cell adhesion. Hydrophobicity, surface charge, surface roughness, material strength, and chemical composition constitute the physical and chemical characteristics of a material.[41] Thus, even though BC/HA and BC/HA/PDA possess different surface chemistry, they both share surface physicochemical characteristics such as hydrophilicity as shown by the FTIR result and surface roughness as shown by the SEM image presented in Figure 3, which directly influenced the morphology and adhesion of MC3T3- E1 cells.

3.5. In Vitro Protein Adsorption. Protein adsorption capacity was investigated in relation to the impact of the surface modification of the BC/HA composite scaffold while using BC as a control. This analysis was conducted to determine the extent to which signaling molecules could be tethered to the BC/HA composite scaffold. The adsorbed quantities per unit area are shown in Figure 8. The efficiency of immobilization by PDA-modified scaffolds was observed to be higher than that of BC/HA and BC at each time point. The first 6 h of incubation for all samples saw a rise in the amount of bovine serum albumin (BSA) adsorbed, with the highest amount of BSA immobilization occurring for BC and BC/HA composite scaffold at 74 and 113 $\mu g \, cm^{-2}$, respectively. Protein adsorption on BC and BC/HA was saturated at 6 h; however,
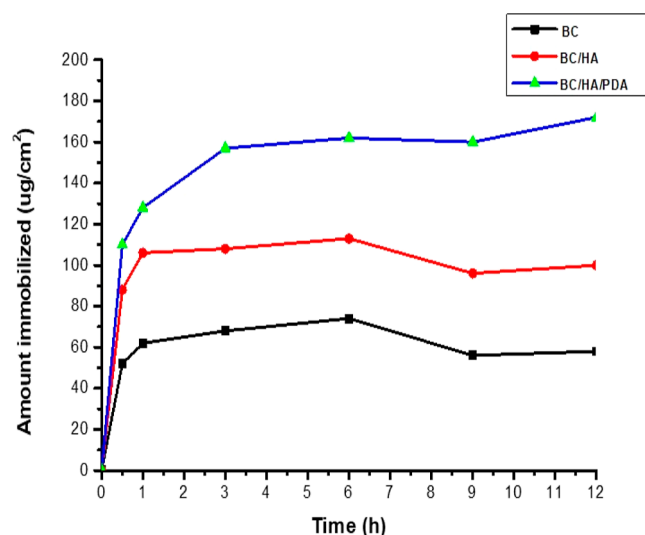
Figure 8. BSA adsorption kinetics of composite scaffolds compared to BC.

the PDA-modified scaffold's adsorption capacity maintained its increase, reaching its maximum ($172\ \mu g\ cm^{-2}$) at 12 h. The increase in protein adsorption in BC/HA and BC/HA/PDA compared to BC could be attributed to the addition of new adsorption sites from HA and PDA. HA is reported to bind to proteins via electrostatic interactions between the calcium cations and the carboxyl anions as well as the phosphate anions and the ammonia cations,[42] while PDA interacts covalently via its *o*-benzoquinone group with the amine group of the BSA.[43] However, PDA has an abundance of functional groups that provide additional active sites capable of covalently binding with BSA and may be responsible for the steady increase in BSA immobilization on PDA-modified scaffolds when compared to the others. Thus, PDA modification of BC/HA composite scaffolds proved to be more efficient in protein adsorption than the unmodified scaffolds.

4. CONCLUSIONS

This study reported the fabrication of a PDA-modified BC-based scaffold using sugarcane filter cake-derived hydroxyapatite (HA) as a component. The physicochemical properties of the prepared HA revealed its similarity to the natural bone mineral, and the nanoparticles were observed to be well dispersed in the cross-section of the composite scaffolds. Dopamine polymerization on the BC/HA composite scaffold was confirmed by surface chemistry analysis, and the impact of reaction time on PDA film formation was additionally identified. The PDA-modified scaffolds also contained a variety of amine active sites that are essential for effective protein interactions. The scaffolds showed no cellular toxicity and are biocompatible with MC3T3-E1 preosteoblasts. In vitro protein adsorption analysis showed that the PDA-modified BC/HA composite scaffolds were more efficient in protein adsorption compared with the unmodified scaffolds. These results demonstrate that agro-industrial biomass residues have the potential to be used in biomedical applications, offering the opportunity to develop highly efficient biomedical devices from sustainable materials. PDA-modified BC and sugarcane filter cake-derived HA composite scaffolds are promising biomaterials for bone tissue engineering.

5. EXPERIMENTAL SECTION

5.1. Bacterial Cellulose Production and Purification.
BC was produced according to Usawattanakul et al.[44] with modifications. *Komagateibacter xylinus* was cultured in 90 mL of coconut water supplemented with sucrose at 5% (w/v) and 2.5% (w/v) of ammonium sulfate at pH 4.5. *K. xylinus* suspensions were aliquoted into 24 well plates and left under static conditions at room temperature for 7 days to produce BC. The cellulose pellicles obtained were washed by boiling several times in deionized water and then treated with a 1% (w/v) sodium hydroxide solution for 1 h. The pellicles were subsequently boiled in deionized water to attain a neutral pH.

5.2. Hydroxyapatite Preparation and Polydopamine-Coated Composite Scaffold Fabrication.
Sugarcane filter cake-derived HA was synthesized as reported in our previous study.[9] Purified BC pellicles were immersed in an HA suspension and left for 15 h under continuous agitation at 200 rpm. Each sample was then briefly immersed in water to remove nonabsorbed HA particles. The pellicles were then lyophilized for subsequent use and referred to in this report as BC/HA. PDA coating was carried out according to Firoozi and Kang[45] with modifications. BC/HA composites were incubated in a dopamine hydrochloride solution ($2\ mg\ mL^{-1}$), prepared with Tris-HCl buffer (pH 8.5), kept in an orbital shaker, and shaken at 150 rpm at 37 °C for 15 h. The PDA-coated scaffolds were then rinsed to remove unreacted PDA and samples were denoted by BC/HA/PDA.

5.3. Physicochemical Characterizations.
5.3.1. X-ray Scattering. XRD patterns of the prepared hydroxyapatite were obtained in the 2θ range of 5 to 70° using an X-ray diffractometer (Bruker D8 ADVANCE, Germany) at a scanning rate of $2°\ min^{-1}$ and operating at a voltage of 40 kV.

WAXS was carried out at the Synchrotron Light Research Institute (Beamline 1.3), Thailand. The samples were exposed to an X-ray of wavelength 0.137 nm for 60 s, at room temperature and a sample to detector distance of 205 mm. The raw data were preprocessed by the SAXSIT program which was used to generate 1D curves. The 1D curves of BC/HA and BC/HA/PDA composite scaffolds were compared with those of pristine BC.

5.3.2. XPS. The elemental composition and oxidation states of the composite scaffolds were analyzed using an XPS PHI5000 VersaProbe II (ULVAC-PHI, Japan) at the SUT-NANOTEC-SLRI Joint Research Facility, Synchrotron Light Research Institute (SLRI), Thailand. A monochromatized A1 Kα X-ray source ($h\nu$ = 1486.6 eV) was utilized to excite the samples. The XPS spectra were fitted by using PHI MultiPak XPS software with a combination of Gaussian−Lorentzian lines. A Shirley-type background was used to remove the background from the spectrum before the peak fitting. The wide-scan spectra were recorded with an energy step of 1.000 eV, while the high-resolution spectra were recorded with an energy step of 0.05 eV and a pass energy of 46.95 eV.

5.3.3. FTIR Spectroscopy. The intermolecular interactions between the components of the scaffolds were analyzed using FTIR spectroscopy (Bruker model: TENSOR 27). Infrared spectra were recorded over a scanning range of 4000−500 cm^{-1} with a resolution of 4 cm^{-1} using the attenuated total reflectance mode.

5.3.4. Scanning Electron Microscopy. The surface appearance and microstructure of the fabricated scaffolds were observed by using a scanning electron microscope (FEI

5.4. Cell Viability and Biocompatibility. The cytotoxicity of BC/HA and BC/HA/PDA composite scaffolds was determined by using sample extracts according to the International Standard Organization (ISO/EN 10993-5). Sample extracts were prepared by incubating samples (BC/HA and BC/HA/PDA) in alpha MEM supplemented with 10% FBS and 1% penicillin−streptomycin for 24 h at 37 °C in a 5% CO_2 atmosphere. MC3T3-E1 preosteoblast cells (57,000 cells/well) were seeded in a 24-well plate and incubated for 24 h at 37 °C in a 5% CO_2 atmosphere. The culture medium was then replaced with sample extracts 24 h post seeding, and the cells were incubated for another 24 h at 37 °C in a 5% CO_2 atmosphere. All samples were sterilized in PBS containing 1% penicillin−streptomycin for 2 h and then preincubated in alpha MEM supplemented with 10% FBS and 1% penicillin−streptomycin for an hour before the test was carried out. The metabolic activity of cells was measured using 3-(4,5-dimethylthiazol-2-yl)-5-(3-carboxymethoxyphenyl)-2-(4-sulfophenyl)-2H-tetrazolium and phenazine methosulfate (MTS) assay according to the manufacturer's protocol. Live/dead cell staining was carried out to obtain a qualitative representation of the cell viability using Calcein AM/ethidium homodimer-(III)(PromoKine), according to the manufacturer's instructions. Stained cells were observed using a fluorescence microscope.

Cell morphology on BC/HA and BC/HA/PDA was determined using SEM as described in the previous Section 5.3.4. Samples were sterilized in PBS containing 1% penicillin−streptomycin for 2 h and then preincubated in alpha MEM supplemented with 10% FBS and 1% penicillin−streptomycin for 30 min before the test was carried out. MC3T3-E1 preosteoblast cells (33,000 cells/cm^2) were seeded on the various scaffolds and incubated at 37 °C and 5% CO_2 atmosphere for 24 h. The scaffolds were thoroughly washed using PBS, fixed with 4% glutaraldehyde, and kept at 4 °C for 24 h. Subsequently, the scaffolds were rinsed once more to get rid of the glutaraldehyde solution and then dehydrated in 30, 50, 70, 90%, and absolute ethanol (repeated three times for 10 min). The scaffolds were then dried by using a critical point dryer and imaged.

5.5. In Vitro Protein Adsorption. BSA was used as a model protein to study the adsorption properties of the BC/HA and BC/HA/PDA composite scaffolds. BSA solution 0.5 (mg mL^{-1}) was prepared, and the various scaffolds were immersed in the solution and incubated at 4 °C for 12 h while studying the rate of immobilization at different times. The bicinchoninic acid assay was used for the quantification of the immobilized proteins by determining the decreasing concentration of the BSA solution.

ASSOCIATED CONTENT

Data Availability Statement

The raw/processed data that support the findings of this study are available from the corresponding author upon request. The data are not publicly available because they are associated with pending work yet to be completed.

AUTHOR INFORMATION

Corresponding Author

 Prakit Sukyai − *Cellulose for Future Materials and Technologies Special Research Unit, Department of Biotechnology, Kasetsart University, Chatuchak, Bangkok 10900, Thailand; Center for Advanced Studies for Agriculture and Food (CASAF), Kasetsart University Institute for Advanced Studies, Kasetsart University, Chatuchak, Bangkok 10900, Thailand;* orcid.org/0000-0003-3602-7208; Email: fagipks@ku.ac.th

Authors

 Mark-Jefferson Buer Boyetey − *Cellulose for Future Materials and Technologies Special Research Unit, Department of Biotechnology, Kasetsart University, Chatuchak, Bangkok 10900, Thailand*

 Nuntaporn Kamonsutthipaijit − *Synchrotron Light Research Institute (Public Organization) 111 University Avenue, Nakhon Ratchasima 30000, Thailand;* orcid.org/0000-0001-5889-1510

 Supinya Nijpanich − *Synchrotron Light Research Institute (Public Organization) 111 University Avenue, Nakhon Ratchasima 30000, Thailand*

 Narong Chanlek − *Synchrotron Light Research Institute (Public Organization) 111 University Avenue, Nakhon Ratchasima 30000, Thailand*

Complete contact information is available at:
https://pubs.acs.org/10.1021/acsomega.3c07266

Notes

The authors declare no competing financial interest.

ACKNOWLEDGMENTS

REFERENCES

(1) Cuadrado-Osorio, P. D.; Ramírez-Mejía, J. M.; Mejía-Avellaneda, L. F.; Mesa, L.; Bautista, E. J. Agro-industrial residues for microbial bioproducts: A key booster for bioeconomy. *Bioresour. Technol. Rep.* **2022**, *20*, 101232. 2022/12/01/

(2) Freitas, L. C.; Barbosa, J. R.; da Costa, A. L. C.; Bezerra, F. W. F.; Pinto, R. H. H.; Carvalho Junior, R. N. d. From waste to sustainable industry: How can agro-industrial wastes help in the development of new products? *Resour. Conserv. Recycl.* **2021**, *169*, 105466. 2021/06/01/

(3) Sadh, P. K.; Duhan, S.; Duhan, J. S. Agro-industrial wastes and their utilization using solid state fermentation: a review. *Bioresources and Bioprocessing*; Springer, 2018; Vol. 5 (1), p 1.

(4) Tripathi, N.; Hills, C. D.; Singh, R. S.; Atkinson, C. J. Biomass waste utilisation in low-carbon products: harnessing a major potential resource. *npj Clim. Atmos. Sci.* **2019**, *2* (1), 35. 2019/10/14

(5) Li, Y.-C. E. Sustainable Biomass Materials for Biomedical Applications. *ACS Biomater. Sci. Eng.* **2019**, *5* (5), 2079−2092. 2019/05/13

(6) Sriwong, C.; Boonrungsiman, S.; Sukyai, P. Sugarcane bagasse cellulose-based scaffolds incorporated hydroxyapatite for promoting proliferation, adhesion and differentiation of osteoblasts. *Ind. Crops Prod.* **2023**, *192*, 115979. 2023/02/01/

(7) Lam, N. T.; Chollakup, R.; Smitthipong, W.; Nimchua, T.; Sukyai, P. Utilizing cellulose from sugarcane bagasse mixed with poly(vinyl alcohol) for tissue engineering scaffold fabrication. *Ind. Crops Prod.* **2017**, *100*, 183−197. 2017/06/01/

(8) Nayar, S.; Guha, A. Waste utilization for the controlled synthesis of nanosized hydroxyapatite. *Mater. Sci. Eng. C* **2009**, *29* (4), 1326−1329. 2009/05/05/

(9) Buer Boyetey, M.-J.; Torgbo, S.; Sukyai, P.; Watthanasakphuban, N.; Kamonsutthipaijit, N. Filter cake-derived calcium carbonate polymorphs from sugar refinery for hydroxyapatite production as a sustainable material for biomedical application. *Ceram. Int.* **2023**, *49*, 23417−23425.

(10) Buer Boyetey, M.-J.; Torgbo, S.; Sukyai, P. Bio-scaffold for bone tissue engineering with focus on bacterial cellulose, biological materials for hydroxyapatite synthesis and growth factors. *Eur. Polym. J.* **2023**, *194*, 112168.

(11) Bhat, S.; Uthappa, U. T.; Altalhi, T.; Jung, H.-Y.; Kurkuri, M. D. Functionalized Porous Hydroxyapatite Scaffolds for Tissue Engineering Applications: A Focused Review. *ACS Biomater. Sci. Eng.* **2022**, *8* (10), 4039−4076. 2022/10/10

(12) Wang, S.-S.; Han, Y.-H.; Ye, Y.-X.; Shi, X.-X.; Xiang, P.; Chen, D.-L.; Li, M. Physicochemical characterization of high-quality bacterial cellulose produced by Komagataeibacter sp. strain W1 and identification of the associated genes in bacterial cellulose production. *RSC Adv.* **2017**, *7* (71), 45145−45155.

(13) Yingkamhaeng, N.; Intapan, I.; Sukyai, P. Fabrication and Characterisation of Functionalised Superparamagnetic Bacterial Nanocellulose Using Ultrasonic-Assisted In Situ Synthesis. *Fibers Polym.* **2018**, *19* (3), 489−497. 2018/03/01

(14) Fredi, G.; Simon, F.; Sychev, D.; Melnyk, I.; Janke, A.; Scheffler, C.; Zimmerer, C. Bioinspired Polydopamine Coating as an Adhesion Enhancer Between Paraffin Microcapsules and an Epoxy Matrix. *ACS Omega* **2020**, *5* (31), 19639−19653. 2020/08/11

(15) Ryu, J. H.; Messersmith, P. B.; Lee, H. Polydopamine Surface Chemistry: A Decade of Discovery. *ACS Appl. Mater. Interfaces* **2018**, *10* (9), 7523−7540. Mar 7

(16) Vinoth Kumar, K. C.; Jani Subha, T.; Ahila, K.; Ravindran, B.; Chang, S.; Mahmoud, A. H.; Mohammed, O. B.; Rathi, M. Spectral characterization of hydroxyapatite extracted from Black Sumatra and Fighting cock bone samples: A comparative analysis. *Saudi J. Biol. Sci.* **2021**, *28* (1), 840−846. 2021/01/01/

(17) Kojima, S.; Nakamura, H.; Lee, S.; Nagata, F.; Kato, K. Hydroxyapatite Formation on Self-Assembling Peptides with Differing Secondary Structures and Their Selective Adsorption for Proteins. *Int. J. Mol. Sci.* 2019, *20*(18), 4650.. https://www.mdpi.com/1422-0067/20/18/4650.

(18) Qi, M.-l.; Wu, Y.; Sun, C.; Zhang, H.; Yao, S. Citrate-Assisted One-Pot Hydrothermal Preparation of Carbonated Hydroxyapatite Microspheres. *Crystals* 2023, *13*(4), 551.. https://www.mdpi.com/2073-4352/13/4/551.

(19) Chang, C.; Skillen, N.; Nagarajan, S.; Ralphs, K.; Irvine, J. T. S.; Lawton, L.; Robertson, P. K. J. Using cellulose polymorphs for enhanced hydrogen production from photocatalytic reforming. *Sustain. Energy Fuels* **2019**, *3* (8), 1971−1975.

(20) Aguayo, M. G.; Fernandez Perez, A.; Reyes, G.; Oviedo, C.; Gacitua, W.; Gonzalez, R.; Uyarte, O. Isolation and Characterization of Cellulose Nanocrystals from Rejected Fibers Originated in the Kraft Pulping Process. *Polymers* **2018**, *10* (10), 1145.

(21) Saska, S.; Barud, H. S.; Gaspar, A. M.; Marchetto, R.; Ribeiro, S. J.; Messaddeq, Y. Bacterial cellulose-hydroxyapatite nanocomposites for bone regeneration. *Int. J. Biomater.* **2011**, *2011*, 1−8.

(22) Coy, E.; Iatsunskyi, I.; Colmenares, J. C.; Kim, Y.; Mrówczyński, R. Polydopamine Films with 2D-like Layered Structure and High Mechanical Resilience. *ACS Appl. Mater. Interfaces* **2021**, *13* (19), 23113−23120. 2021/05/19

(23) Godoy-Gallardo, M.; Portolés-Gil, N.; López-Periago, A. M.; Domingo, C.; Hosta-Rigau, L. Multi-layered polydopamine coatings for the immobilization of growth factors onto highly-interconnected

and bimodal PCL/HA-based scaffolds. *Mater. Sci. Eng. C* **2020**, *117*, 111245. 2020/12/01/

(24) Bykov, G.; Abkhalimov, E.; Ershov, V.; Ershov, B. Radiolysis of Portland cement and magnesium phosphate cement: Effect of the content and state of water on the Physicochemical properties and the mechanism and kinetics of hydrogen formation. *Radiat. Phys. Chem.* **2022**, *190*, 109822.

(25) Wang, G.; Zhang, J.; Lin, S.; Xiao, H.; Yang, Q.; Chen, S.; Yan, B.; Gu, Y. Environmentally friendly nanocomposites based on cellulose nanocrystals and polydopamine for rapid removal of organic dyes in aqueous solution. *Cellulose* **2020**, *27*, 2085−2097.

(26) Liao, Y.; Weng, Y.; Wang, J.; Zhou, H.; Lin, J.; He, S. Silicone rubber composites with high breakdown strength and low dielectric loss based on polydopamine coated mica. *Polymers* **2019**, *11* (12), 2030.

(27) Uskoković, V. X-ray photoelectron and ion scattering spectroscopic surface analyses of amorphous and crystalline calcium phosphate nanoparticles with different chemical histories. *Phys. Chem. Chem. Phys.* **2020**, *22* (10), 5531−5547. Mar 11

(28) Gopinath, C. S.; Hegde, S. G.; Ramaswamy, A. V.; Mahapatra, S. Photoemission studies of polymorphic CaCO3 materials. *Mater. Res. Bull.* **2002**, *37* (7), 1323−1332. 2002/06/01/

(29) Liu, Q.; Li, J.; Zhou, Z.; Xie, J.; Lee, J. Y. Hydrophilic Mineral Coating of Membrane Substrate for Reducing Internal Concentration Polarization (ICP) in Forward Osmosis. *Sci. Rep.* **2016**, *6* (1), 19593.

(30) Dreghici, D. B.; Butoi, B.; Predoi, D.; Iconaru, S. L.; Stoican, O.; Groza, A. Chitosan-Hydroxyapatite Composite Layers Generated in Radio Frequency Magnetron Sputtering Discharge: From Plasma to Structural and Morphological Analysis of Layers. *Polymers* **2020**, *12* (12), 3065.

(31) Bai, J.; Nagashima, T.; Yajima, T. XPS study of apatite formed from simulated body fluid on a titanium substrate surface nitrided by an atmospheric pressure nitrogen microwave plasma. *J. Photopolym. Sci. Technol.* **2015**, *28* (3), 455−459.

(32) Huang, Z.-H.; Peng, S. W.; Hsieh, S. L.; Kirankumar, R.; Huang, P. F.; Chang, T. M.; Dwivedi, A. K.; Chen, N. F.; Wu, H. M.; Hsieh, S. Polydopamine ultrathin film growth on mica via in-situ polymerization of dopamine with applications for silver-based antimicrobial coatings. *Materials* **2021**, *14* (3), 671.

(33) Hemmatpour, H.; De Luca, O.; Crestani, D.; Stuart, M. C. A.; Lasorsa, A.; van der Wel, P. C. A.; Loos, K.; Giousis, T.; Haddadi-Asl, V.; Rudolf, P. New insights in polydopamine formation via surface adsorption. *Nat. Commun.* **2023**, *14* (1), 664. 2023/02/07

(34) Lopes, T. D.; Riegel-Vidotti, I. C.; Grein, A.; Tischer, C. A.; Faria-Tischer, P. C. Bacterial cellulose and hyaluronic acid hybrid membranes: Production and characterization. *Int. J. Biol. Macromol.* **2014**, *67*, 401−408. Jun

(35) Sheng, W.; Li, B.; Wang, X.; Dai, B.; Yu, B.; Jia, X.; Zhou, F. Brushing up from "anywhere" under sunlight: a universal surface-initiated polymerization from polydopamine-coated surfaces. *Chem. Sci.* **2015**, *6* (3), 2068−2073.

(36) Saleh, A. K.; Tolba, E.; Salama, A. In situ development of bacterial cellulose/hydroxyapatite nanocomposite membrane based on two different fermentation strategies: characterization and cytotoxicity evaluation. *Biomass Conversion and Biorefinery*; Springer, 2023.

(37) Coelho, F.; Cavicchioli, M.; Specian, S. S.; Scarel-Caminaga, R. M.; Penteado, L. d. A.; Medeiros, A. I. d.; Ribeiro, S. J. d. L.; Capote, T. S. d. O. Bacterial cellulose membrane functionalized with hydroxiapatite and anti-bone morphogenetic protein 2: A promising material for bone regeneration. *PLoS One* **2019**, *14* (8), No. e0221286.

(38) Kopeć, K.; Wojasiński, M.; Ciach, T. Superhydrophilic polyurethane/polydopamine nanofibrous materials enhancing cell adhesion for application in tissue engineering. *Int. J. Mol. Sci.* **2020**, *21* (18), 6798.

(39) Xu, Z.; Wang, N.; Liu, P.; Sun, Y.; Wang, Y.; Fei, F.; Zhang, S.; Zheng, J.; Han, B. Poly(Dopamine) Coating on 3D-Printed Poly-

Lactic-Co-Glycolic Acid/β-Tricalcium Phosphate Scaffolds for Bone Tissue Engineering. *Molecules* **2019**, *24* (23), 4397.

(40) Collins, K.; Gates, E.; Gilchrist, C.; Hoffman, B. Bio-instructive cues in scaffolds for musculoskeletal tissue engineering and regenerative medicine. *Bio-Instructive Scaffolds for Musculoskeletal Tissue Engineering and Regenerative Medicine*; Elsevier, 2017; pp 3−35.

(41) Hsin, I. C.; Yiwei, W. Cell Responses to Surface and Architecture of Tissue Engineering Scaffolds. In *Regenerative Medicine and Tissue Engineering*; Daniel, E., Ed.; IntechOpen: Rijeka, 2011; p 27.

(42) Swain, S. K.; Sarkar, D. Study of BSA protein adsorption/ release on hydroxyapatite nanoparticles. *Appl. Surf. Sci.* **2013**, *286*, 99−103. 2013/12/01/

(43) Zhu, L.-P.; Jiang, J.-H.; Zhu, B.-K.; Xu, Y.-Y. Immobilization of bovine serum albumin onto porous polyethylene membranes using strongly attached polydopamine as a spacer. *Colloids Surf., B* **2011**, *86* (1), 111−118. 2011/08/01/

(44) Usawattanakul, N.; Torgbo, S.; Sukyai, P.; Khantayanuwong, S.; Puangsin, B.; Srichola, P. Development of Nanocomposite Film Comprising of Polyvinyl Alcohol (PVA) Incorporated with Bacterial Cellulose Nanocrystals and Magnetite Nanoparticles. *Polymers*, 2021, *13*(11), 1778.. https://www.mdpi.com/2073-4360/13/11/1778.

(45) Firoozi, N.; Kang, Y. Immobilization of FGF on Poly(xylitol dodecanedioic Acid) Polymer for Tissue Regeneration. *Sci. Rep.* **2020**, *10* (1), 10419. Jun 26